LETTER

Simultaneous Low-Order Phase Suppression and Defect Passivation for Efficient and Stable Blue Light-Emitting Diodes

Zhenwei Ren, Ling Li, Jiahao Yu, Ruiman Ma, Xiangtian Xiao, Rui Chen,* Kai Wang,* Xiao Wei Sun, Wan-Jian Yin, and Wallace C. H. Choy*

Read Online

ACCESS | Metrics & More | Article Recommendations | Supporting Information

ABSTRACT: Quasi-two-dimensional (quasi-2D) perovskite is rising as a promising luminescent material for blue perovskite light-emitting diodes (PeLEDs). However, typical quasi-2D perovskites show a wide distribution of low-order phases and low efficiency owing to the inefficient energy transfer. Meanwhile, the defects and traps generated during the perovskite crystallization increase nonradiative recombination, further aggravating the external quantum efficiency (EQE). Herein, we demonstrate a unique quasi-2D perovskite with low-order phase suppression and defect passivation for efficient energy transfer and light emission by incorporating a 2D perovskite and an excess ammonium salt into the quasi-2D perovskite solution. By optimizing the new class of quasi-2D perovskite, we achieve blue PeLEDs with the brightness of 1765 cd m^{-2}, EQE of 7.51%, low turn-on voltage of 3.07 V, and long operation lifetime of 3961 s under constant driving current without any shift of the electroluminescence spectra. The work contributes to promoting efficient and stable blue PeLEDs.
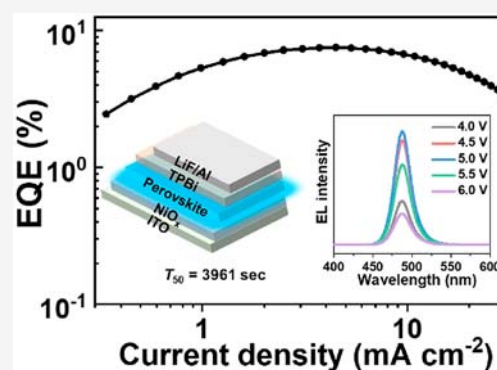
Recently, perovskite light-emitting diodes (PeLEDs) have emerged as attractive optoelectronic devices, benefiting from the promising properties of perovskites including tunable light emission color, high color purity, and high photoluminescence quantum yields (PLQYs).[1−5] Significant improvements have been achieved in green, red, and near-infrared PeLEDs where impressive external quantum efficiencies (EQEs) exceeding 20% are obtained,[6−8] signaling a great potential toward practical applications. As compared with efficient PeLEDs, only moderate performances were reported for blue PeLEDs,[9−13] which set substantial limitations in the applications of full-color display and solid-state lighting. Therefore, it is highly desirable to realize high-performing blue PeLEDs.

One of the intensively investigated perovskite blue emitters is the inorganic perovskite nanocrystals (NCs) of $CsPbX_3$ where X is bromide, chloride, or mixture of bromide and chloride ions.[14,15] In 2015, the first blue PeLEDs based on the all-inorganic perovskite NCs were reported.[16] However, there are some concerns, such as mass nonradiative defects in the NCs and inefficient charge transport due to insulating organic ligands,[17−19] that tremendously impede the progress of perovskite NC blue PeLEDs. Different approaches have been investigated to improve the performances of NC-based blue

PeLEDs, such as metal ion doping for reducing the nonradiative recombination[20−25] and ligand-exchange incorporation for enhancing carrier transportation.[26,27] Besides the zero-dimensional perovskite NCs, the bromide-based two-dimensional (2D) perovskite nanoplatelets (NPls) with exciton quantum confinement in one dimension were also proven to obtain high PLQY for blue emission.[28−34] However, their PeLED EQEs are normally below 1%, which may be attributed to the inefficient charge injection due to the randomly oriented distribution of the NPls.

Another potential material for blue PeLEDs is quasi-2D perovskites with the general formula of $A_2(BPbX_3)_{n-1}PbX_4$, where A is a long-chain organic ammonium, B an inorganic/organic cation such as Cs^+ or methylammonium (MA^+), and X a halide (e.g., Br, Cl ion).[2,35] The blue emission peaks can be obtained by reducing the stacking number (n) of perovskite
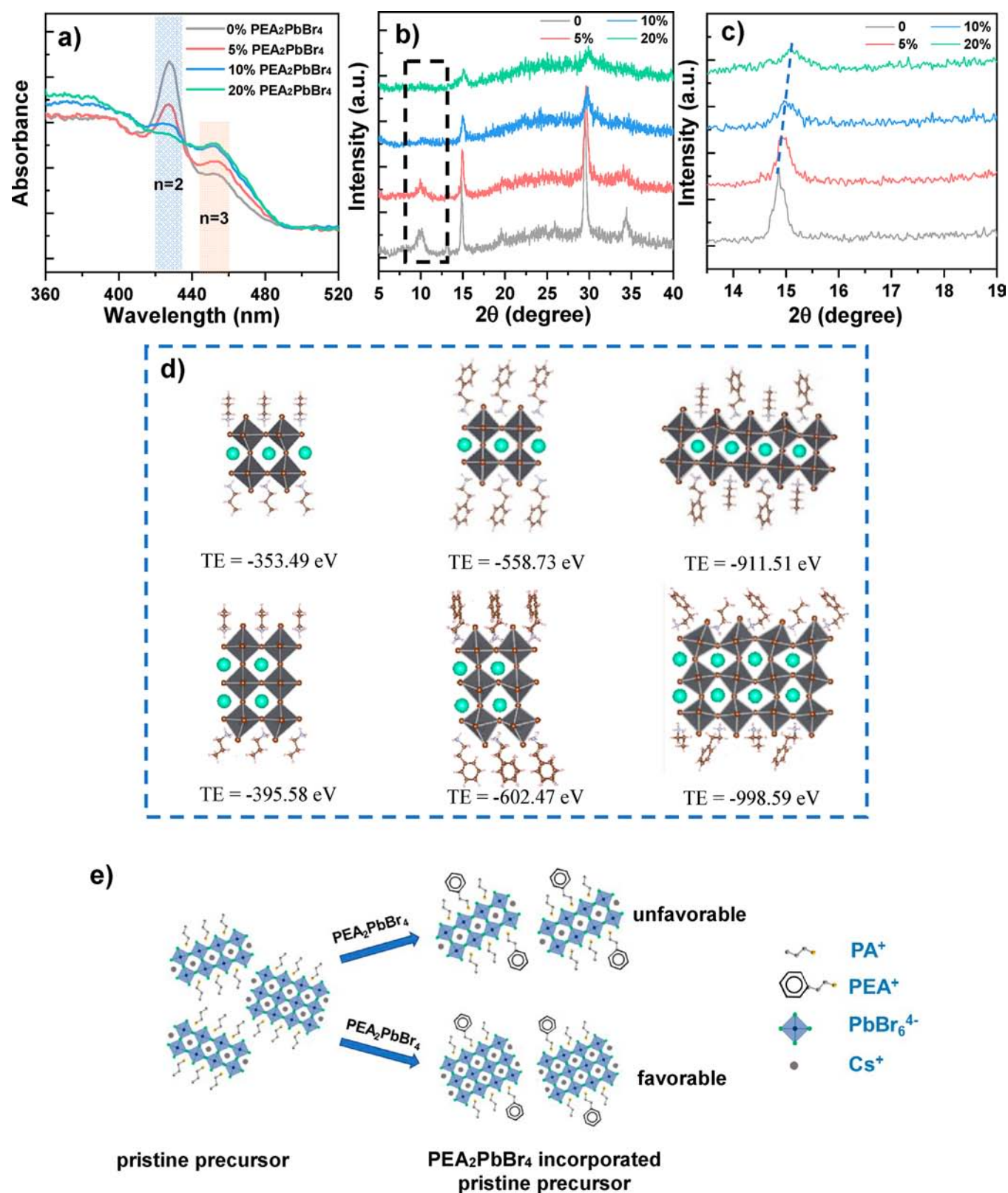
Figure 1. (a) UV–visible absorption spectra of PEA$_2$PbBr$_4$-incorporated perovskite films. (b) XRD measurements for pristine and PEA$_2$PbBr$_4$-incorporated perovskites and (c) the corresponding enlarged peak of the XRD patterns. (d) The crystal structures (n = 2, 3 phases) of PA$^+$, PEA$^+$ single ligand, and PEA$^+$ and PA$^+$ mixed ligands formed quasi-2D perovskites and the corresponding total energies through first-principles calculations. (e) Schematic diagram of the effect of PEA$_2$PbBr$_4$ on the quasi-2D perovskite phases.

unit cells in the formula. Recently, quasi-2D perovskites have emerged as efficient luminescent materials for high-performing blue PeLEDs.[36−43] For example, the mixed halides of Br and

Cl together with the cation of PEA were employed to make PEA$_2$Cs$_{n−1}$Pb$_n$(Cl$_x$Br$_{1−x}$)$_{3n+1}$ quasi-2D perovskites, which were then assembled with the optimized thickness of PEDOT:PSS

to modulate the position of the recombination zone for high device performances at emission wavelength of 480 nm with an EQE of 5.7% and a luminance of 3780 cd m^{-2}.[38] However, the electroluminescence (EL) red-shifted at high bias voltage because of phase separation caused by the migration of the halides. In order to improve the EL spectral stability, the strategy of rubidium−cesium alloyed "A-site" were combined to construct PEA$_2$(Rb$_x$Cs$_{1-x}$)$_2$Pb$_3$Br$_{10}$ PeLEDs. The devices show stable EL spectra with a half-lifetime of 14.5 min and an EQE of 1.35% at 476 nm.[39] Subsequently, a cocktail strategy of multication (Cs/Rb/FA/PEA/K)Pb(Cl/Br)$_3$ was proposed and demonstrated for excellent stability of blue PeLEDs.[40] Then, an efficient blue EL from PeLEDs of quantum-confined perovskite nanoparticles embedded within the mixed-phase quasi-2D quantum was well boosted, with the EQE reaching 9.5%.[41] Very recently, yttrium(III) chloride was reported to incorporate into the perovskite's grain surface for increased bandgap of grain shell which can confine the charge carriers for efficient radiative recombination, and a high efficiency performance of 11.0% was achieved in the PeLEDs.[42] Different from bulk and quantum dot PeLED counterparts, the electrons and holes injected into the large bandgap phase of quasi-2D perovskite in PeLEDs, i.e., low-n phase with fewer perovskite layers, will transfer to the small bandgap phase, i.e., large-n phase with more perovskite layers. They will recombine in large-n phase and emit as photons.[44] It is also known that quasi-2D perovskites usually contain a variety of n species as mixed phases, especially the low-n phase quasi-2D perovskites which would result in low emission efficiency owing to the inefficient internal energy transfer.[39,45,46] Therefore, fine modulation of the phases for high phase purity and thus for efficient energy transfer in quasi-2D perovskite is vital for high-efficiency emission.[43,44] Meanwhile, inevitable defects and traps will be generated during crystallization of quasi-2D perovskite prepared via solution-processing methods, which will increase the chance for nonradiative recombination and thus low emission efficiency.

In this work, we propose an approach of incorporating a quasi-2D perovskite solution with a 2D perovskite and an excess ammonium salt to synthesize a new class of quasi-2D perovskites. The new perovskites show interesting features of phase redistribution through the low-n (low-order) phase suppression for efficient energy transfer and defect passivation with the trap density reduction of over 60% for diminishing the nonradiative recombination. We also experimentally and theoretically investigate the roles of the incorporated materials on the quasi-2D perovskites. After optimizing the new qausi-2D perovskites, we achieve PeLEDs with very good EQE of 7.51%, high brightness of 1765 cd m^{-2}, and very low turn-on voltage of 3.07 V, representing one of the most efficient blue PeLEDs reported. Notably, the blue PeLEDs show an ultralong operational stability of 3961 s under continuous constant driving current. In particular, the EL spectra stay unchanged without any peak shift monitored during the entire stability test, showing properties superior to those of reported blue PeLEDs and thus contributing to high-efficiency and -stability blue PeLEDs.

The synthesis starts with propylamine hydrobromide (PABr) as the organic ammonium salt which has been proven to be good precursor material in our previous work.[47] The precursor solution of PA$_2$(CsPbBr$_3$)$_{n-1}$PbBr$_4$ quasi-2D perovskite was prepared by dissolving PABr and CsPbBr$_3$ perovskite into DMSO, in which CsPbBr$_3$ perovskite was synthesized through the reported facile chemical precipitation method.[6] In contrast, we strategically introduce 2D PEA$_2$PbBr$_4$ into quasi-2D PA$_2$(CsPbBr$_3$)$_{n-1}$PbBr$_4$ perovskite solution to form a PA$^+$ and PEA$^+$ mixed ligand system and transform the quasi-2D perovskite into a new perovskite of PEA$_x$PA$_{2-x}$(CsPbBr$_3$)$_{n-1}$PbBr$_4$ (0 ≤ x < 2) with low-order phase suppression. Details are discussed in the Supporting Information. The roles, explanation, and verification of PEA$_2$PbBr$_4$ are studied in detail as follows.

Regarding the optical properties of perovskite, Figure 1a shows UV−visible absorption spectra of the perovskite films incorporated with different amounts of PEA$_2$PbBr$_4$. When there is no PEA$_2$PbBr$_4$ incorporation, distinct excitonic absorption peaks appear at wavelengths of 428 and 452 nm corresponding to n = 2 and n = 3 phases in the quasi-2D perovskites. In contrast, when PEA$_2$PbBr$_4$ concentration increases from 0 to 20%, there is an obvious variation of the excitonic absorption properties (Figure 1a). The excitonic absorption peak at 428 nm (corresponding to n = 2 phase) continuously weakens in increasing PEA$_2$PbBr$_4$ concentration. Ultimately, it is hard to observe the n = 2 absorption peak at the concentration of 20%, showing the phase-modulation role of PEA$_2$PbBr$_4$ on the quasi-2D perovskites. To further confirm the phase modulation role of PEA$_2$PbBr$_4$, we investigate the effects of PEABr and PbBr$_2$ on the quasi-2D perovskites (see Figure S2). It is found that neither PEABr nor PbBr$_2$ can induce phase evolution between n = 2 to n = 3 of the quasi-2D perovskite, while such perovskite phase evolution can be achieved by incorporating PEA$_2$PbBr$_4$, stressing its importance in the distinct phase evolution. Additionally, the X-ray diffraction (XRD) measurements in Figure 1b show that the diffraction peak at 10.01° corresponding to the low-order (i.e., n = 2) phase[48] (shown in Figure S3) gradually reduces when PEA$_2$PbBr$_4$ concentration increases and disappear when PEA$_2$PbBr$_4$ content reaches 20%. Moreover, we find the peak slightly shifts toward higher angles from 14.86° to 15.05° (Figure 1c), which can be assigned to the n = 2 and n = 3 phase with the layer lattice constant (d) of 17.7 and 23.5 Å, respectively (Table S1). We further performed grazing incident X-ray diffraction (GIXRD) measurements of pristine and PEA$_2$PbBr$_4$-incorporated quasi-2D perovskites to collect more information on the thin perovskite films (Figure S4 and Table S2). The results unveil the evolution of low-n (i.e., n = 2) phase to large-n phase (i.e., n = 3) in the perovskite films with the presence of PEA$_2$PbBr$_4$ as further verified with the following transient absorption spectroscopy.

We then fundamentally investigate the effects of organic cation ligands on perovskite phase formation after incorporation of PEA$_2$PbBr$_4$ into the perovskite. The first-principles total energy (TE) calculations have been performed to characterize the thermodynamic stability of the mixed ligands constructed perovskites (Figure 1d). The energy difference (ΔE) is expressed in the formula $\Delta E = E_{mix} - (E_{PEA} + E_{PA})$, where E_{mix}, E_{PEA}, and E_{PA} are the TEs of PEA$^+$ and PA$^+$ mixed ligands, PEA$^+$, and PA$^+$ single ligand formed quasi-2D perovskites, respectively, in which the positive (negative) sign of ΔE indicates the unstable (stable) nature of the system. It is found that in the n = 2 phase, E_{mix} is −911.51 eV, which is larger than the sum of E_{PEA} (−558.73 eV) and E_{PA} (−353.49 eV), and positive ΔE is obtained for the n = 2 mixed ligand system. While E_{mix} of the n = 3 phase is −998.59 eV, which is smaller than the sum of the corresponding E_{PEA} (−602.47 eV) and E_{PA} (−395.58 eV), leading to negative ΔE for the n = 3

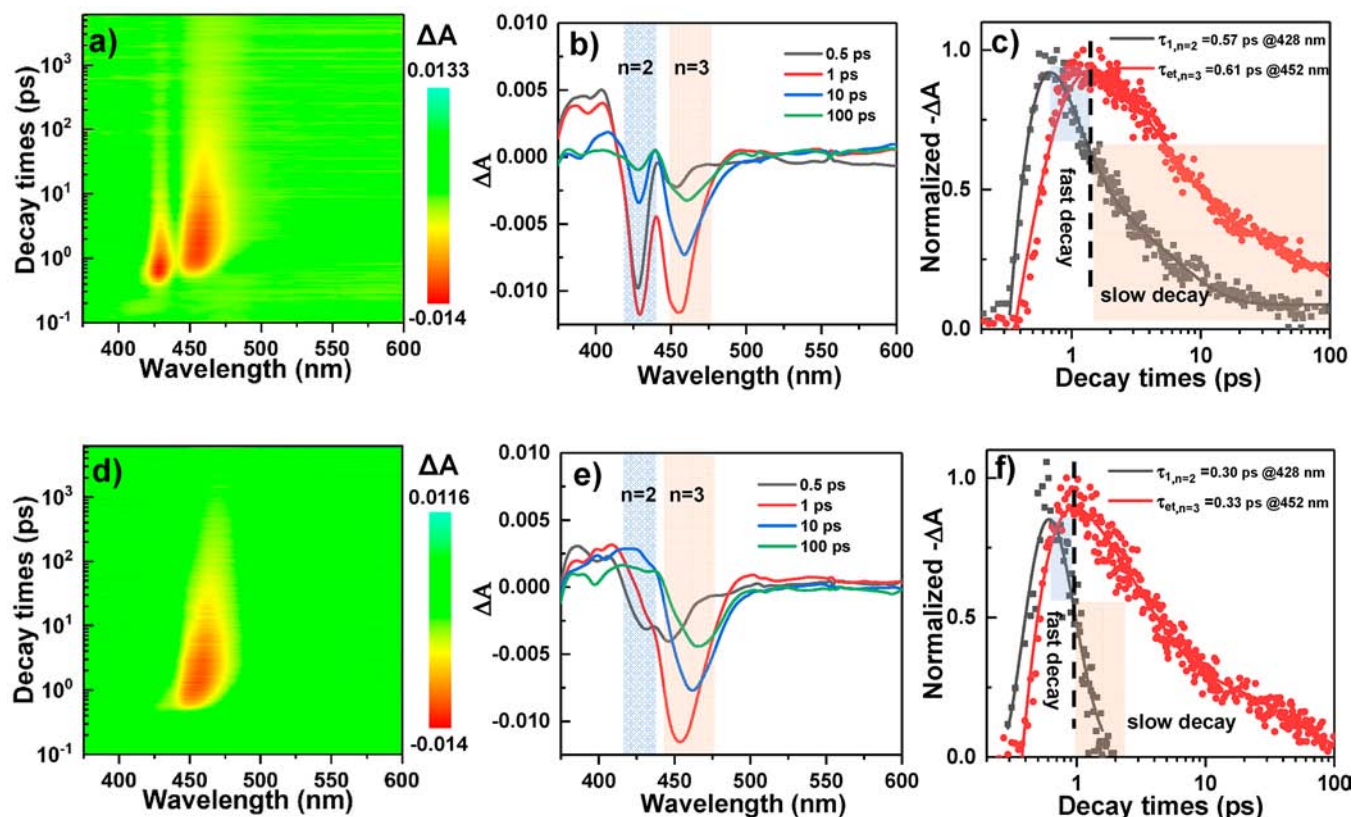Figure 2. TA measurements for pristine (a−c) and PEA$_2$PbBr$_4$-incorporated (d−f) perovskites. (a and d) TA time decay spectrograms; (b and e) TA spectra at different probe delay times; and (c and f) TA kinetics probed at selected wavelengths for pristine and PEA$_2$PbBr$_4$-incorporated perovskite films, respectively.

mixed ligand system. The results show the $n = 2$ phase is thermodynamically unstable in the mixed ligands system while the conversion from a single PA$^+$ ligand to a PA$^+$ and PEA$^+$ mixed ligand system is favorable for the $n = 3$ phase. This is consistent with the analysis of GIXRD patterns (Figure S4 and Table S2), where the signal of the $n = 3$ mixed ligand phase is observed while no signal of the $n = 2$ mixed ligand phase is found in the PEA$_2$PbBr$_4$-incorporated perovskite. Consequently, we have successfully experimentally demonstrated the PEA$_2$PbBr$_4$-incorporated perovskite with low-order phase suppression and theoretically proved the preferentially formed $n = 3$ mixed ligand phase from the proposed approach.

To gain further insight into the transfer and recombination dynamics of photogenerated carriers in the pristine perovskite and PEA$_2$PbBr$_4$-incorporated perovskite, transient absorption spectroscopy has been used for characterization. Figure 2 shows the transient absorption (TA) characterizations of the samples at room temperature. As shown in Figure 2a, two distinctive ground-state photobleaching (PB) signals corresponding to $n = 2$ and $n = 3$ phases can be clearly observed in pristine perovskites. This indicates the two dominant phases in pristine quasi-2D perovskites, which are consistent with the steady-state absorption spectra. Figure 2b shows the TA spectra of pristine perovskites at different delay times. It is found that photogenerated carriers are principally generated in both the $n = 2$ and $n = 3$ phases at the initial stage. Because of the quantum confinement effect, the quasi-2D perovskite with larger n value will have a smaller bandgap. Therefore, the energy transfer can be expected if the two phases coexist in the materials. This can be verified by the TA signal. At a longer

decay time, the signal related to the $n = 2$ phase decreases while the $n = 3$ species increases, which indicates the energy transfer from $n = 2$ to $n = 3$ perovskite phase.[49,50] To further study the carrier-transfer process, time traces at selected probe wavelengths (428 and 452 nm corresponding to $n = 2$ and $n = 3$ species) are extracted as shown in Figure 2c. The kinetics of each PB can be well-fitted by a multiexponential function: $\Delta A(t) = a_1 \exp(-t/\tau_1) + a_2 \exp(-t/\tau_2) + a_3 \exp(-t/\tau_3) - c_1 \exp(-t/\tau_{et})$, where a_1, a_2, a_3, and c_1 are amplitudes; τ_1 is the fast decay time constant ascribed to the energy-transfer process in the perovskite; τ_2 and τ_3 represent the slow decay constant due to complex decay processes such as trap-assisted recombination; and τ_{et} is the formation time constant,[39,51] which are extracted and listed in Table S3. The PB of $n = 2$ phase shows a fast decay component with τ_1 of 0.57 ps. Coincidentally, the τ_{et} fitted from the raising component of the PB of $n = 3$ phase is 0.61 ps, within the time scale of τ_1 showing a fast energy-transfer process in picoseconds. In addition, we also study the effect of excitation laser intensity on the energy-transfer process in TA kinetics (Figure S6 and Table S4). It is observed that the τ_1 value varies in a little range with the increase of the laser power intensity from 5 to 45 μJ cm^{-2}, indicating the energy-transfer process is only slighted affected by the excitation power range. However, the values of τ_2 and τ_3 decrease obviously when increasing the laser power, which is likely ascribed to the increased Auger recombination at higher excitation density.[52]

In contrast, for PEA$_2$PbBr$_4$-incorporated perovskites, a strong PB peak around 452 nm can be found (Figure 2d), which indicates the dominant $n = 3$ phase in the quasi-2D
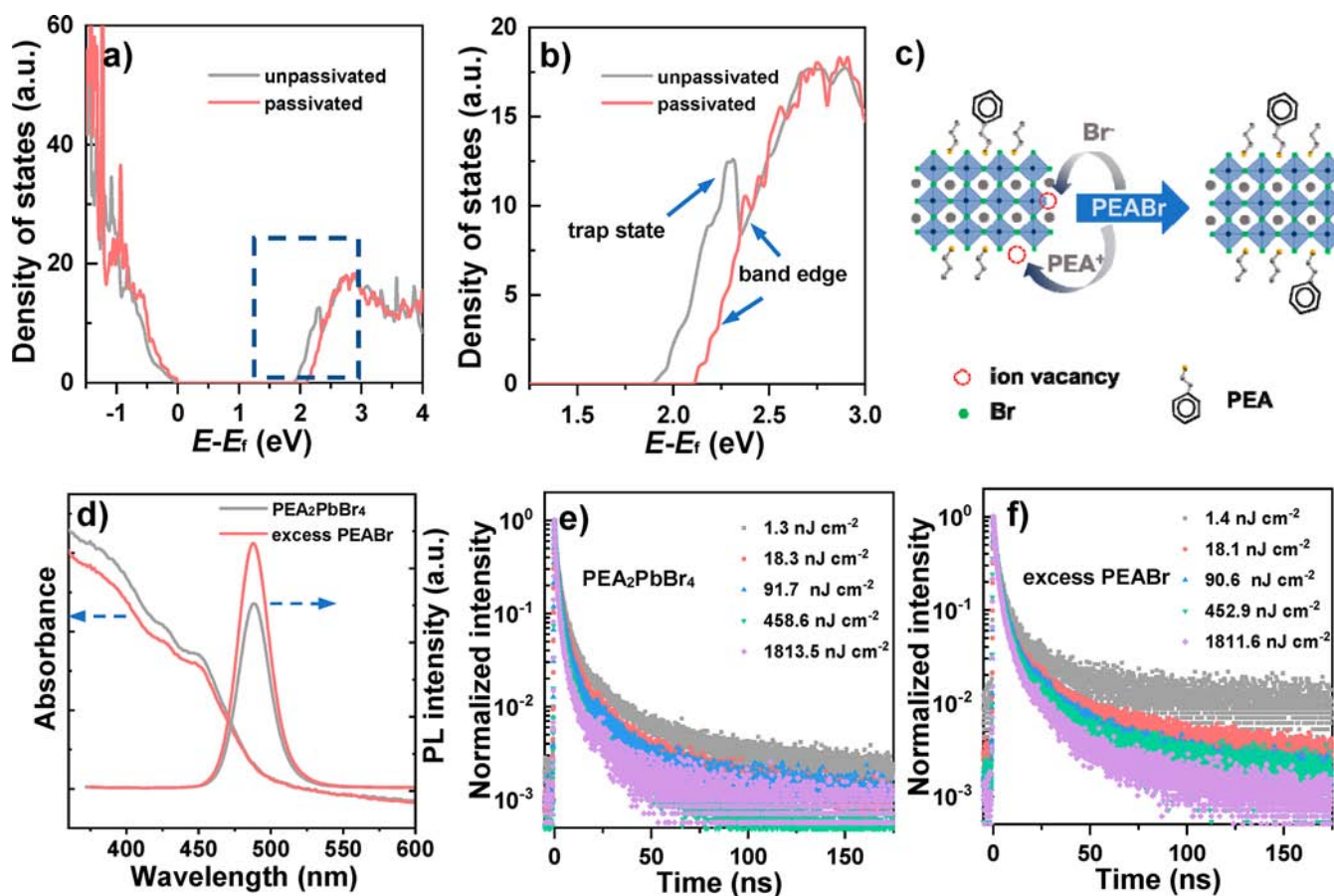
Figure 3. Density of states (DOS) and optical properties of PEA_2PbBr_4-incorporated perovskites with and without excess PEABr decoration: (a) Density of states (DOS), (b) the magnified DOS extracted from panel a, and (c) schematic diagram of the passivation role of excess PEABr within the quasi-2D perovskites. (d) UV−visible absorption spectra and the corresponding PL spectra. Time-resolved PL spectra under different excitation intensities of (e) PEA_2PbBr_4 and (f) excess PEABr-incorporated perovskite films.

perovskites. In addition, a very weak signal of the $n = 2$ phase at a short decay time can be observed, which is greatly weakened as compared to the pristine perovskite (Figure S7). This also implies that the low-order phases (particularly $n = 2$ phase) can be remarkably suppressed after PEA_2PbBr_4 modulation. As shown in Figure 2e, it is found that the decay time of the $n = 2$ phase in the PEA_2PbBr_4-incorporated perovskites is much faster than that in pristine perovskite. To further confirm the fast decay time, the probed time trace of $n = 2$ phase is extracted (Figure 2f), in which the decay time constant of τ_1 decreases from 0.57 ps (pristine) to 0.30 ps. This implies more efficient energy transfer from a wider bandgap phase ($n = 2$) to a narrow one ($n = 3$). The more efficient energy transfer can be further verified by the reduced τ_{et} of $n = 3$ phase (0.33 ps) for PEA_2PbBr_4-incorporated perovskites, which is faster than that of pristine (0.61 ps) perovskites. Consequently, the data obtained by the ultrafast laser spectroscopy shows that the phases in quasi-2D perovskites can be transformed from mixed phases of $n = 2$, 3 to the low-order phase ($n = 2$) suppressed qusai-2D perovskite by the incorporation of PEA_2PbBr_4, which facilitates efficient energy transfer from the large bandgap phase to the small one without blocking of the adjacent large bandgap phases in the perovskites (Figure S8). The effective phase control ascribed to the PEA_2PbBr_4 incorporation is consistent with the optical characterizations shown in Figure 1, which implies the successful suppression of low-order phase ($n = 2$)

after the modification. This is the main reason for the enhanced device performance, as will be discussed later.

During the synthesis of the new quasi-2D perovskite, we strategically passivate the quasi-2D perovskite by incorporating excess PEABr. The PEA_2PbBr_4-incorporated perovskites show high trap state density of 3.85×10^{17} cm^{-3} (Figure S9) which will increase the chance for nonradiative recombination and result in limited emission efficiency. We find that the introduction of an excess amount of PEABr can effectively passivate perovskite defects as described in the Supporting Information. As we know, inevitable defects are generated during the perovskite crystallization owing to the ionic nature of hybrid perovskites. Although the origin of the defects is not very clear, they are widely believed to be related to the ionic defects such as halide and ammonium vacancies.[53] We theoretically confirm the role of passivation from studying the density of sates (DOS) of the perovskites (Figure S10). The DOS of the unpassivated perovskite shows a distinct trap state around the band edge due to the ion vacancies within the perovskite (Figure 3a). Interestingly, the ion vacancies can be annihilated by passivation of excess PEABr, which can provide both bromide and ammonium ions to fill the vacancy sites for the ionic compensation (Figure 3c). Consequently, the distinct trap states are eliminated in the excess PEABr-decorated perovskite (Figure 3b), indicating its good defect passivation for the perovskite.
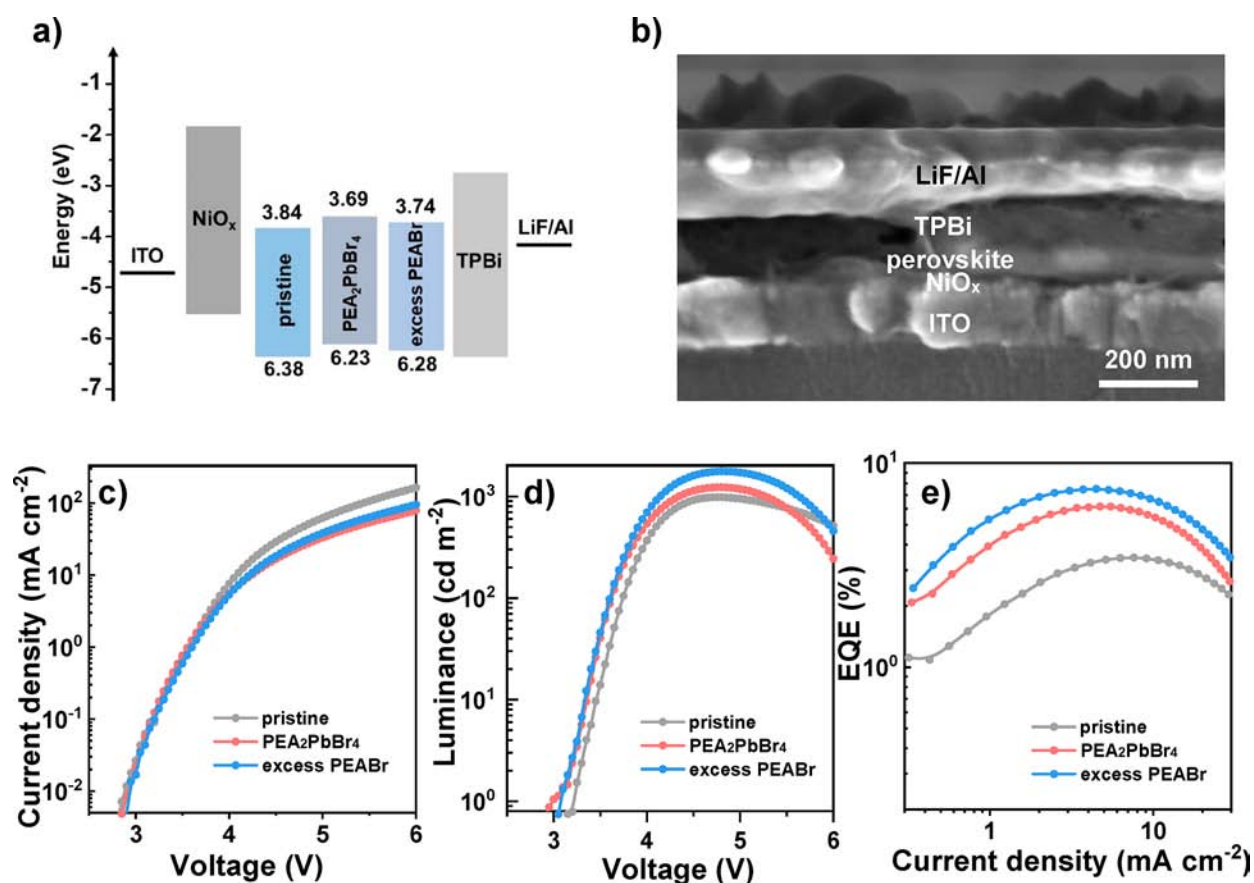
Figure 4. Perovskite light-emitting diode structure and performance. (a) Energy levels for different layers of the device; (b) cross-sectional SEM image of the PeLEDs; and (c) current density−voltage (J−V), (d) luminance−voltage (L−V), and (e) EQE characterizations of the corresponding PeLEDs.

Experimentally, the defect passivation is further verified by the dramatic enhancement in the PL intensity as shown in Figure 3d. The PLQY increases from 39.5% (without PEABr decoration) to 49.6% (with 5% excess PEABr decoration), which illustrates the defect passivation role of PEABr for a large reduction of nonradiative recombination. To further verify the passivation effect of PEABr and study the carrier recombination processes, the time-resolved PL (TRPL) spectra under different excitation intensities have been measured as shown in Figure 3e,f. The decays are fitted by biexponential curves, in which the fast and slow decay components correspond to the trap-assisted recombination and radiative recombination, respectively.[54−56] The extracted parameters of the decay process are plotted in Figure S11e,f. It is revealed that both the fast and slow decay lifetimes for the excess PEABr-decorated perovskite are much longer than that without excess PEABr-decorated perovskite. Besides, the lifetime variations with the amount of the excess PEABr have also been studied (Figure S12). It is found that the average lifetime improves notably with increase of the PEABr concentration (Table S5). The results vividly confirm the effective passivation role of PEABr for fewer defects, such that the trap state density of excess PEABr-decorated perovskite can be dramatically reduced to 1.43×10^{17} cm^{-3} from 3.85×10^{17} cm^{-3} (without excess PEABr decoration) (Figure S9). Besides passivating perovskite defects, the PEABr will not change the phase of the perovskite. Our results show that there is no shift of the absorption edge upon the decoration of excess PEABr. In addition, the ratio of the peak intensity between $n =$

2 and $n = 3$ phases is 1.13 and remains the same after the decoration of PEABr (see Figure 3d). Furthermore, no new XRD peak appears in the quasi-2D perovskite after the decoration of PEABr (see Figure S13). Consequently, we demonstrate that the introduction of an excess amount of PEABr will not only passivate the perovskite defects but also maintain the perovskite phase. The efficient passivation role of PEABr will be a promising approach for high-performing PeLEDs as discussed in the following.

We fabricate PeLEDs with a structure of ITO/NiO$_x$/perovskite/TPBi/LiF/Al, in which NiO$_x$ is utilized as the hole injection layer (HIL) for the good hole injection properties,[47,57,58] TPBi the electron injection layer (EIL), and quasi-2D perovskites the emission layer. The energy bands of pristine, PEA$_2$PbBr$_4$-incorporated, and excess PEABr-decorated perovskites were determined by ultraviolet photoelectron spectroscopy (UPS) (Figure S14), which are summarized in Figure 4a. As compared with the pristine perovskite, the energy band of PEA$_2$PbBr$_4$-incorporated and excess PEABr-decorated perovskite films are slightly increased and thus benefit the improving of hole injection and bring down the turn-on voltage of PeLEDs. The thicknesses of the HIL, emission layer, EIL, and LiF/Al layers are 24, 55, 70, and 130 nm, respectively, as measured from the cross-sectional scanning electron microscopy (SEM) image in Figure 4b. The device performances in Figure 4d show that the maximum brightness (L_{max}) of pristine PeLEDs is 982 cd m^{-2} at a bias of 4.75 V, which increases to 1231 cd m^{-2} for the PEA$_2$PbBr$_4$-incorporated device at the same bias (Table 1). Similarly, the

Table 1. Device Performance of Pristine, PEA$_2$PbBr$_4$, and Excess PEABr-Decorated PeLEDs

device	V_{th} (V)	L_{max} (cd m^{-2})	EQE (%)
pristine	3.22	982	3.46
PEA$_2$PbBr$_4$	2.98	1231	6.15
excess PEABr	3.07	1765	7.51

EQE increases from 3.46% (pristine) to 6.15% (PEA$_2$PbBr$_4$-incorporated) (Figure 4e). The improvement is mainly attributed to the efficient energy transport of the PEA$_2$PbBr$_4$-incorporated perovskite (as shown in Figure 2). It is also noted that the turn-on voltage (V_{th}, corresponding with luminance of 1 cd m^{-2}) of PEA$_2$PbBr$_4$-incorporated PeLEDs (2.98 V) is lower than that of pristine ones (3.22 V), which is among the lowest turn-on voltages of the reported blue PeLEDs[37−43] owing to the narrowed energy barrier for efficient hole injection (Figure 4a). In addition, in order to study the charge injection and transfer capacity of the PeLEDs, the capacitance−voltage ($C-V$) characteristics are also measured (Figure S15). The capacitance improves with the increase of bias voltage, and the carriers are injected into the perovskites. In other words, the capacitance of PEA$_2$PbBr$_4$-incorporated PeLEDs is larger than that of pristine device at the same bias up to the voltage value of 3.4 V, and thus more charges are injected. At higher bias, the capacitance sharply declines in the PEA$_2$PbBr$_4$-incorporated case because of the largely reduced

carriers caused by the large radiative recombination of electrons and holes.[59] While compared with pristine PeLEDs, the lower peak capacitance is observed for PEA$_2$PbBr$_4$-incorporated device, which indicates more charge-transfer capacity in PEA$_2$PbBr$_4$-incorporated perovskite because of suppression of the low-order phase. To further study the effects of PEA$_2$PbBr$_4$, the PeLED performance with different incorporated PEA$_2$PbBr$_4$ concentrations is investigated, as shown in Figure S16. The devices achieve the best performance at the PEA$_2$PbBr$_4$ concentration of 10%. The higher concentration of PEA$_2$PbBr$_4$ (such as the concentration of 15% and 20%) will reduce the device performance because of the high induced trap states (Figure S17, S18). Consequently, by incorporating an appropriate amount of PEA$_2$PbBr$_4$ into qusai-2D perovskite, the performances of PeLEDs can be improved.

By introduction of excess PEABr to passivate the PEA$_2$PbBr$_4$-incorporated perovskites, the PeLED performances are further enhanced with the luminance improved from 1231 cd m^{-2} (without excess PEABr decoration) to 1765 cd m^{-2} (with PEABr decoration). Notably, a high EQE of 7.51% is also achieved for excess PEABr-decorated PeLEDs, which is among the highest for blue PeLEDs.[36−43] In addition, the excess PEABr-decorated PeLEDs also show good reproducibility with EQE of 6.39% averaged from 20 devices (Figure S19). This enhancement is mainly attributed to the largely reduced defects in the perovskite films by over 60% as
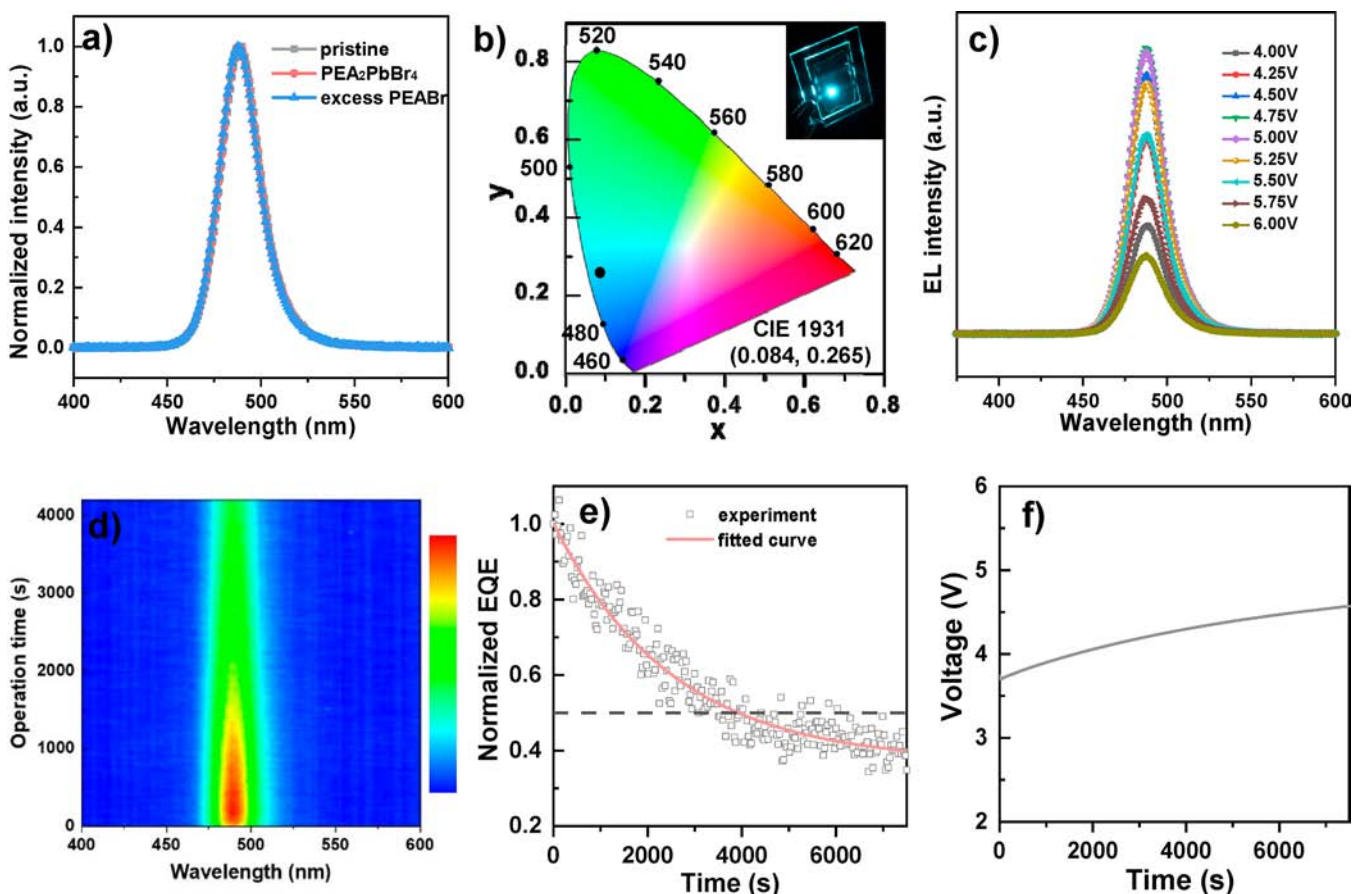

Figure 5. EL properties of the PeLEDs. (a) EL spectra of pristine, PEA$_2$PbBr$_4$-incorporated, and excess PEABr-decorated blue PeLEDs. (b) CIE coordinate of excess PEABr-decorated PeLEDs with the emission image in the inset and the corresponding EL spectra (c) at different biased voltages and (d) under continuous constant current of 1.5 mA cm^{-2}. (e) Time-dependent stability lifetime measurements of excess PEABr-decorated PeLEDs with constant current and (f) the corresponding bias voltage traces during the lifetime test.

compared to the undecorated perovskite (Figure S9). In addition, we also study the hysteresis of PEA_2PbBr_4 and excess PEABr-decorated PeLEDs (Figure S20). It is found that the PEA_2PbBr_4-incorporated PeLEDs show obvious hysteresis for both current density and luminance with scanning from the forward to reverse direction. Nevertheless, the devices with excess PEABr show reduced hysteresis due to the passivation role of PEABr for fewer defects and thus less ion migration. Meanwhile, a lower efficiency roll-off is also observed for excess PEABr-decorated PeLEDs (Figure S21). Although the origin of the large bandgap PeLED efficiency roll-off is not very clear, it is likely associated with the Auger recombination, because it is observed that the PL lifetime decreases at high excitation intensities for PEA_2PbBr_4 and excess PEABr-decorated perovskites (Figure S11).[60,61] The device performance with different PEABr concentrations is also studied as shown in Figure S23, in which the PeLED with 5% PEABr shows the highest EQE, and the performance begins to decline at higher concentrations owing to the induced low hole injection rate of the PeLEDs (Figure S24).

From the EL spectra of PeLEDs as shown in Figure 5a, the peaks centered at 488 nm are obtained for PEA_2PbBr_4 and excess PEABr-decorated PeLEDs, which are consistent with their PL spectra assigned to the recombination center of $n \geq 4$ phase (Figure S4) because of the energy funneling effect in quasi-2D perovskite. This implies that the EL is generated merely from the perovskite layer because of the strong confinement of the injected carriers within quasi-2D perovskites. The excess PEABr-decorated PeLEDs show a narrowband emission with the full width at half-maximum (fwhm) of around 25 nm and thus a good color purity with Commission Internationale de L'Eclairage (CIE) chromaticity coordinate at (0.084, 0.265) (Figure 5b). The CIE chromaticity coordinates of pristine and PEA_2PbBr_4-incorporated PeLEDs are also shown in Figure S25. It is known that the spectral stability is an important index to evaluate the PeLEDs toward practical applications and is a challenging issue of quasi-2D blue PeLEDs, possibly because of ion migration under voltage bias and phase instability with Joule heating or moist conditions.[62,63] The EL spectra of excess PEABr-decorated PeLEDs under different bias voltages are measured as shown in Figure 5c. It is found that the EL intensity increases when the bias voltage increases from 4.0 to 4.75 V and then declines at higher bias. Under different bias, the EL peak wavelength (488 nm) and fwhm (~25 nm) remain unchanged. This implies that the excess PEABr-decorated PeLED has very good spectral stability.

As we know, LEDs are usually current driven devices; we now turn to the lifetime tests of the devices under continuous constant current driving. The EL spectra under continuous driving current are shown in Figure 5d. It is noted that the peak positions remain at 488 nm upon extending the operation time, revealing an excellent spectral stability during operation. The lifetime of the devices measured under continuous constant current (1.5 mA cm^{-2} corresponding to the initial EQE of 6.02%) is recorded in Figure 5e. A very impressive lifetime T_{50} (defined as the elapsed time of LED decaying to 50% of its initial EQE) of 3961 s is achieved for the excess PEABr-decorated PeLEDs, which is one of the most stable blue PeLEDs.[36-43] The bias voltages during the lifetime measurements are also shown in Figure 5f, in which the slopes increase monotonically with the stress time increasing as the device resistance increases during operation. In addition,

lifetime measurements of the devices measured under large injection current density of 10 and 20 mA cm^{-2} were also carried out to show the potential practical applications of the PeLEDs (Figure S26). It is observed that the lifetime decreases rapidly under large injection current density, and the monitored lifetimes of 296 and 174 s are obtained at 10 and 20 mA cm^{-2}, respectively. Although the lifetimes are shortened at large injection current density, the peak positions stay unchanged, indicating a good spectral stability during operation. We also study the lifetimes of the pristine and PEA_2PbBr_4-incorporated PeLEDs, as shown in Figure S27. The lifetimes are 496 and 1611 s with initial EQE of 2.87% and 5.03%, respectively, lagging far behind that of the excess PEABr-decorated PeLEDs. Consequently, our results show that the excess PEABr-decorated PeLEDs show excellent spectral stability and exhibit the longest lifetime for blue PeLEDs, which promote the quasi-2D perovskite LEDs toward practical applications.

In summary, we demonstrate an efficient quasi-2D perovskite blue emitter of $PEA_xPA_{2-x}(CsPbBr_3)_{n-1}PbBr_4$ with simultaneous phase redistribution and defect passivation for high-performing and stable blue quasi-2D PeLEDs. The new quasi-2D perovskite is realized by incorporation of PEA_2PbBr_4 and an excess PEABr into quasi-2D perovskite $(PA_2(CsPbBr_3)_{n-1}PbBr_4)$ solution. The PEA_2PbBr_4-incorporated quasi-2D perovskite LEDs promote an efficient energy-transfer process from the low-n phase to the high-n phase perovskites and thus improve device performance with the EQE increased from 3.46% (pristine) to 6.15% (PEA_2PbBr_4-incorporated). We the further introduce the passivation of excess PEABr into the PEA_2PbBr_4-incorporated perovskites which remarkably reduces the trap state density by over 60%. Eventually, the excess PEABr-decorated PeLEDs show an efficient EQE of 7.51% and a high brightness of 1765 cd m^{-2} with a very low turn-on voltage of 3.07 V. It is noted that the devices reveal an excellent operation stability with an ultralong lifetime T_{50} of 3961 s under continuous constant driving current. In particular, the EL spectra are very stable without any peak shift during the entire stability test, signaling a great potential for the blue PeLEDs toward practical applications.

■ ASSOCIATED CONTENT

Ⓢ Supporting Information

The Supporting Information is available free of charge at https://pubs.acs.org/doi/10.1021/acsenergylett.0c01015.

Experimental section including materials, device fabrication, and characterizations; optical properties; electrical characteristics; theoretical calculation; and device performanceof blue PeLEDs (PDF)

■ AUTHOR INFORMATION

Corresponding Authors

Rui Chen − *Department of Electrical and Electronic Engineering, Southern University of Science and Technology, Shenzhen 518055, China;* ⓞ orcid.org/0000-0002-0445-7847; Email: chenr@sustech.edu.cn

Kai Wang − *Department of Electrical and Electronic Engineering, Southern University of Science and Technology, Shenzhen 518055, China;* ⓞ orcid.org/0000-0003-0443-6955; Email: wangk@sustc.edu.cn

Wallace C. H. Choy − *Department of Electrical and Electronic Engineering, The University of Hong Kong, Hong Kong, China;*

orcid.org/0000-0002-9535-4076; Email: chchoy@eee.hku.hk

Authors

Zhenwei Ren − *Department of Electrical and Electronic Engineering, The University of Hong Kong, Hong Kong, China*

Ling Li − *College of Energy, Soochow Institute for Energy and Materials InnovationS (SIEMIS) Jiangsu Provincial Key Laboratory for Advanced Carbon Materials and Wearable Energy Technologies, Soochow University, Suzhou 215006, China*

Jiahao Yu − *Department of Electrical and Electronic Engineering, Southern University of Science and Technology, Shenzhen 518055, China*

Ruiman Ma − *Department of Electrical and Electronic Engineering, The University of Hong Kong, Hong Kong, China*

Xiangtian Xiao − *Department of Electrical and Electronic Engineering, The University of Hong Kong, Hong Kong, China*

Xiao Wei Sun − *Department of Electrical and Electronic Engineering, Southern University of Science and Technology, Shenzhen 518055, China;* orcid.org/0000-0002-2840-1880

Wan-Jian Yin − *College of Energy, Soochow Institute for Energy and Materials InnovationS (SIEMIS) Jiangsu Provincial Key Laboratory for Advanced Carbon Materials and Wearable Energy Technologies, Soochow University, Suzhou 215006, China;* orcid.org/0000-0003-0932-2789

Complete contact information is available at:
https://pubs.acs.org/10.1021/acsenergylett.0c01015

Notes

The authors declare no competing financial interest.

■ **REFERENCES**

(1) Yuan, M.; Quan, L. N.; Comin, R.; Walters, G.; Sabatini, R.; Voznyy, O.; Hoogland, S.; Zhao, Y.; Beauregard, E. M.; Kanjanaboos, P.; Lu, Z.; Kim, D. H.; Sargent, E. H. Perovskite Energy Funnels for Efficient Light-emitting Diodes. *Nat. Nanotechnol.* **2016**, *11*, 872−877.

(2) Chen, Y.; Sun, Y.; Peng, J.; Tang, J.; Zheng, K.; Liang, Z. 2D Ruddlesden−Popper perovskites for optoelectronics. *Adv. Mater.* **2018**, *30*, 1703487.

(3) Veldhuis, S. A.; Boix, P. P.; Yantara, N.; Li, M.; Sum, T. C.; Mathews, N.; Mhaisalkar, S. G. Perovskite Materials for Light-emitting Diodes and Lasers. *Adv. Mater.* **2016**, *28*, 6804−6834.

(4) Protesescu, L.; Yakunin, S.; Bodnarchuk, M. I.; Krieg, F.; Caputo, R.; Hendon, C. H.; Yang, R. X.; Walsh, A.; Kovalenko, M. V. Nanocrystals of Cesium Lead Halide Perovskites (CsPbX$_3$, X = Cl, Br, and I): Novel Optoelectronic Materials Showing Bright Emission with Wide Color Gamut. *Nano Lett.* **2015**, *15*, 3692−3696.

(5) Richter, J. M.; Abdi-Jalebi, M.; Sadhanala, A.; Tabachnyk, M.; Rivett, J. P. H.; Pazos-Outón, L. M.; Gödel, K. C.; Price, M.; Deschler, F.; Friend, R. H. Enhancing Photoluminescence Yields in Lead Halide Perovskites by Photon Recycling and Light Out-Coupling. *Nat. Commun.* **2016**, *7*, 13941.

(6) Lin, K.; Xing, J.; Quan, L. N.; Pelayo García de Arquer, F.; Gong, X.; Lu, J.; Xie, L.; Zhao, W.; Zhang, D.; Yan, C.; Li, W.; Liu, X.; Lu, Y.; Kirman, J.; Sargent, E. H.; Xiong, Q.; Wei, Z. Perovskite Light-Emitting Diodes with External Quantum Efficiency Exceeding 20%. *Nature* **2018**, *562*, 245−248.

(7) Cao, Y.; Wang, N.; Tian, H.; Guo, J.; Wei, Y.; Chen, H.; Miao, Y.; Zou, W.; Pan, K.; He, Y.; Cao, H.; Ke, Y.; Xu, M.; Wang, Y.; Yang, M.; Du, K.; Fu, Z.; Kong, D.; Dai, D.; Jin, Y.; Li, G.; Li, H.; Peng, Q.; Wang, J.; Huang, W. Perovskite Light-Emitting Diodes Based on Spontaneously Formed Submicrometre-Scale Structures. *Nature* **2018**, *562*, 249−253.

(8) Zhao, B.; Bai, S.; Kim, V.; Lamboll, R.; Shivanna, R.; Auras, F.; Richter, J. M.; Yang, L.; Dai, L.; Alsari, M.; She, X.-J.; Liang, L.; Zhang, J.; Lilliu, S.; Gao, P.; Snaith, H. J.; Wang, J.; Greenham, N. C.; Friend, R. H.; Di, D. High-Efficiency Perovskite−Polymer Bulk Heterostructure Light-Emitting Diodes. *Nat. Photonics* **2018**, *12*, 783−789.

(9) Xing, J.; Zhao, Y.; Askerka, M.; Quan, L. N.; Gong, X.; Zhao, W.; Zhao, J.; Tan, H.; Long, G.; Gao, L.; Yang, Z.; Voznyy, O.; Tang, J.; Lu, Z.-H.; Xiong, Q.; Sargent, E. H. Color-Stable Highly Luminescent Sky-Blue Perovskite Light-Emitting Diodes. *Nat. Commun.* **2018**, *9*, 3541.

(10) Wang, Q.; Ren, J.; Peng, X.-F.; Ji, X.-X.; Yang, X.-H. Efficient Sky-Blue Perovskite Light-Emitting Devices Based on Ethylammonium Bromide Induced Layered Perovskites. *ACS Appl. Mater. Interfaces* **2017**, *9*, 29901−29906.

(11) Chen, Z.; Zhang, C.; Jiang, X.-F.; Liu, M.; Xia, R.; Shi, T.; Chen, D.; Xue, Q.; Zhao, Y.-J.; Su, S.; Yip, H.-L.; Cao, Y. High-Performance Color-Tunable Perovskite Light Emitting Devices through Structural Modulation from Bulk to Layered Film. *Adv. Mater.* **2017**, *29*, 1603157.

(12) Sadhanala, A.; Ahmad, S.; Zhao, B.; Giesbrecht, N.; Pearce, P. M.; Deschler, F.; Hoye, R. L. Z.; Gödel, K. C.; Bein, T.; Docampo, P.; Dutton, S. E.; De Volder, M. F. L.; Friend, R. H. Blue-Green Color Tunable Solution Processable Organolead Chloride−Bromide Mixed Halide Perovskites for Optoelectronic Applications. *Nano Lett.* **2015**, *15*, 6095−6101.

(13) Congreve, D. N.; Weidman, M. C.; Seitz, M.; Paritmongkol, W.; Dahod, N. S.; Tisdale, W. A. Tunable Light-Emitting Diodes Utilizing Quantum-Confined Layered Perovskite Emitters. *ACS Photonics* **2017**, *4*, 476−481.

(14) Mondal, N.; De, A.; Samanta, A. Achieving Near-Unity Photoluminescence Efficiency for Blue-Violet-Emitting Perovskite Nanocrystals. *ACS Energy Lett.* **2019**, *4*, 32−39.

(15) Shamsi, J.; Urban, A. S.; Imran, M.; De Trizio, L.; Manna, L. Metal Halide Perovskite Nanocrystals: Synthesis, Post-Synthesis Modifications, and Their Optical Properties. *Chem. Rev.* **2019**, *119*, 3296−3348.

(16) Song, J.; Li, J.; Li, X.; Xu, L.; Dong, Y.; Zeng, H. Quantum Dot Light-Emitting Diodes Based on Inorganic Perovskite Cesium Lead Halides (CsPbX$_3$). *Adv. Mater.* **2015**, *27*, 7162−7167.

(17) Huang, H.; Bodnarchuk, M. I.; Kershaw, S. V.; Kovalenko, M. V.; Rogach, A. L. Lead Halide Perovskite Nanocrystals in the Research Spotlight: Stability and Defect Tolerance. *ACS Energy Lett.* **2017**, *2*, 2071−2083.

(18) Li, G.; Wisnivesky Rocca Rivarola, F.; Davis, N. J. L. K.; Bai, S.; Jellicoe, T. C.; de la Peña, F.; Hou, S.; Ducati, C.; Gao, F.; Friend, R. H.; Greenham, N. C.; Tan, Z.-K. Highly Efficient Perovskite Nanocrystal Light-Emitting Diodes Enabled by a Universal Cross-linking Method. *Adv. Mater.* **2016**, *28*, 3528−3534.

(19) Li, J.; Xu, L.; Wang, T.; Song, J.; Chen, J.; Xue, J.; Dong, Y.; Cai, B.; Shan, Q.; Han, B.; Zeng, H. 50-Fold EQE Improvement up to 6.27% of Solution-Processed All-Inorganic Perovskite CsPbBr$_3$ QLEDs via Surface Ligand Density Control. *Adv. Mater.* **2017**, *29*, 1603885.

(20) Zhou, Y.; Chen, J.; Bakr, O. M.; Sun, H.-T. Metal-Doped Lead Halide Perovskites: Synthesis, Properties, and Optoelectronic Applications. *Chem. Mater.* **2018**, *30*, 6589−6613.

(21) Yong, Z.-J.; Guo, S.-Q.; Ma, J.-P.; Zhang, J.-Y.; Li, Z.-Y.; Chen, Y.-M.; Zhang, B.-B.; Zhou, Y.; Shu, J.; Gu, J.-L.; Zheng, L.-R.; Bakr, O. M.; Sun, H.-T. Doping-Enhanced Short-Range Order of Perovskite Nanocrystals for Near-Unity Violet Luminescence Quantum Yield. *J. Am. Chem. Soc.* **2018**, *140*, 9942−9951.

(22) Bi, C.; Wang, S.; Li, Q.; Kershaw, S. V.; Tian, J.; Rogach, A. L. Thermally Stable Copper(II)-Doped Cesium Lead Halide Perovskite Quantum Dots with Strong Blue Emission. *J. Phys. Chem. Lett.* **2019**, *10*, 943−952.

(23) Liu, M.; Zhong, G.; Yin, Y.; Miao, J.; Li, K.; Wang, C.; Xu, X.; Shen, C.; Meng, H. Aluminum-Doped Cesium Lead Bromide Perovskite Nanocrystals with Stable Blue Photoluminescence Used for Display Backlight. *Adv. Sci.* **2017**, *4*, 1700335.

(24) Yao, J.-S.; Ge, J.; Han, B.-N.; Wang, K.-H.; Yao, H.-B.; Yu, H.-L.; Li, J.-H.; Zhu, B.-S.; Song, J.-Z.; Chen, C.; Zhang, Q.; Zeng, H.-B.; Luo, Y.; Yu, S.-H. Ce³⁺-Doping to Modulate Photoluminescence Kinetics for Efficient CsPbBr₃ Nanocrystals Based Light-Emitting Diodes. *J. Am. Chem. Soc.* **2018**, *140*, 3626−3634.

(25) Hou, S.; Gangishetty, M. K.; Quan, Q.; Congreve, D. N. Efficient Blue and White Perovskite Light-Emitting Diodes via Manganese Doping. *Joule* **2018**, *2*, 2421−2433.

(26) Pan, J.; Quan, L. N.; Zhao, Y.; Peng, W.; Murali, B.; Sarmah, S. P.; Yuan, M.; Sinatra, L.; Alyami, N. M.; Liu, J.; Yassitepe, E.; Yang, Z.; Voznyy, O.; Comin, R.; Hedhili, M. N.; Mohammed, O. F.; Lu, Z. H.; Kim, D. H.; Sargent, E. H.; Bakr, O. M. Highly Efficient Perovskite-Quantum-Dot Light-Emitting Diodes by Surface Engineering. *Adv. Mater.* **2016**, *28*, 8718−8725.

(27) Zhang, B.-B.; Yuan, S.; Ma, J.-P.; Zhou, Y.; Hou, J.; Chen, X.; Zheng, W.; Shen, H.; Wang, X.-C.; Sun, B.; Bakr, O. M.; Liao, L.-S.; Sun, H.-T. General Mild Reaction Creates Highly Luminescent Organic-Ligand-Lacking Halide Perovskite Nanocrystals for Efficient Light-Emitting Diodes. *J. Am. Chem. Soc.* **2019**, *141*, 15423−15432.

(28) Hoye, R. L. Z.; Lai, M.-L.; Anaya, M.; Tong, Y.; Gałkowski, K.; Doherty, T.; Li, W.; Huq, T. N.; Mackowski, S.; Polavarapu, L.; Feldmann, J.; MacManus-Driscoll, J. L.; Friend, R. H.; Urban, A. S.; Stranks, S. D. Identifying and Reducing Interfacial Losses to Enhance Color-Pure Electroluminescence in Blue-Emitting Perovskite Nanoplatelet Light-Emitting Diodes. *ACS Energy Lett.* **2019**, *4*, 1181−1188.

(29) Yang, D.; Zou, Y.; Li, P.; Liu, Q.; Wu, L.; Hu, H.; Xu, Y.; Sun, B.; Zhang, Q.; Lee, S.-T. Large-Scale Synthesis of Ultrathin Cesium Lead Bromide Perovskite Nanoplates with Precisely Tunable Dimensions and Their Application in Blue Light-Emitting Diodes. *Nano Energy* **2018**, *47*, 235−242.

(30) Peng, S.; Wang, S.; Zhao, D.; Li, X.; Liang, C.; Xia, J.; Zhang, T.; Xing, G.; Tang, Z. Pure Bromide-Based Perovskite Nanoplatelets for Blue Light-Emitting Diodes. *Small Methods* **2019**, *3*, 1900196.

(31) Wu, Y.; Wei, C.; Li, X.; Li, Y.; Qiu, S.; Shen, W.; Cai, B.; Sun, Z.; Yang, D.; Deng, Z.; Zeng, H. In Situ Passivation of PbBr₆⁴⁻ Octahedra toward Blue Luminescent CsPbBr₃ Nanoplatelets with Near 100% Absolute Quantum Yield. *ACS Energy Lett.* **2018**, *3*, 2030−2037.

(32) Bohn, B. J.; Tong, Y.; Gramlich, M.; Lai, M. L.; Döblinger, M.; Wang, K.; Hoye, R. L. Z.; Müller-Buschbaum, P.; Stranks, S. D.; Urban, A. S.; Polavarapu, L.; Feldmann, J. Boosting Tunable Blue Luminescence of Halide Perovskite Nanoplatelets through Post-synthetic Surface Trap Repair. *Nano Lett.* **2018**, *18*, 5231−5238.

(33) Liang, D.; Peng, Y.; Fu, Y.; Shearer, M. J.; Zhang, J.; Zhai, J.; Zhang, Y.; Hamers, R. J.; Andrew, T. L.; Jin, S. Color-Pure Violet-Light-Emitting Diodes Based on Layered Lead Halide Perovskite Nanoplates. *ACS Nano* **2016**, *10*, 6897−6904.

(34) Deng, W.; Jin, X.; Lv, Y.; Zhang, X.; Zhang, X.; Jie, J. 2D Ruddlesden−Popper Perovskite Nanoplate Based Deep-Blue Light-Emitting Diodes for Light Communication. *Adv. Funct. Mater.* **2019**, *29*, 1903861.

(35) Kumawat, N. K.; Liu, X.-K.; Kabra, D.; Gao, F. Blue Perovskite Light-Emitting Diodes: Progress, Challenges and Future Directions. *Nanoscale* **2019**, *11*, 2109−2120.

(36) Yantara, N.; Jamaludin, N. F.; Febriansyah, B.; Giovanni, D.; Bruno, A.; Soci, C.; Sum, T. C.; Mhaisalkar, S.; Mathews, N. Designing the Perovskite Structural Landscape for Efficient Blue Emission. *ACS Energy Lett.* **2020**, *5*, 1593−1600.

(37) Vashishtha, P.; Ng, M.; Shivarudraiah, S. B.; Halpert, J. E. High Efficiency Blue and Green Light-Emitting Diodes Using Ruddlesden−Popper Inorganic Mixed Halide Perovskites with Butylammonium Interlayers. *Chem. Mater.* **2019**, *31*, 83−89.

(38) Li, Z.; Chen, Z.; Yang, Y.; Xue, Q.; Yip, H.-L.; Cao, Y. Modulation of Recombination Zone Position for Quasi-Two-Dimensional Blue Perovskite Light-Emitting Diodes with Efficiency Exceeding 5%. *Nat. Commun.* **2019**, *10*, 1027.

(39) Jiang, Y.; Qin, C.; Cui, M.; He, T.; Liu, K.; Huang, Y.; Luo, M.; Zhang, L.; Xu, H.; Li, S.; Wei, J.; Liu, Z.; Wang, H.; Kim, G.-H.; Yuan, M.; Chen, J. Spectra Stable Blue Perovskite Light-Emitting Diodes. *Nat. Commun.* **2019**, *10*, 1868.

(40) Yuan, F.; Ran, C.; Zhang, L.; Dong, H.; Jiao, B.; Hou, X.; Li, J.; Wu, Z. A Cocktail of Multiple Cations in Inorganic Halide Perovskite toward Efficient and Highly Stable Blue Light-Emitting Diodes. *ACS Energy Lett.* **2020**, *5*, 1062−1069.

(41) Liu, Y.; Cui, J.; Du, K.; Tian, H.; He, Z.; Zhou, Q.; Yang, Z.; Deng, Y.; Chen, D.; Zuo, X.; Ren, Y.; Wang, L.; Zhu, H.; Zhao, B.; Di, D.; Wang, J.; Friend, R. H.; Jin, Y. Efficient Blue Light-Emitting Diodes Based on Quantum-Confined Bromide Perovskite Nanostructures. *Nat. Photonics* **2019**, *13*, 760−764.

(42) Wang, Q.; Wang, X.; Yang, Z.; Zhou, N.; Deng, Y.; Zhao, J.; Xiao, X.; Rudd, P.; Moran, A.; Yan, Y.; Huang, J. Efficient Sky-Blue Perovskite Light-Emitting Diodes via Photoluminescence Enhancement. *Nat. Commun.* **2019**, *10*, 5633.

(43) Yuan, S.; Wang, Z.-K.; Xiao, L.-X.; Zhang, C.-F.; Yang, S.-Y.; Chen, B.-B.; Ge, H.-T.; Tian, Q.-S.; Jin, Y.; Liao, L.-S. Optimization of Low-Dimensional Components of Quasi-2D Perovskite Films for Deep-Blue Light-Emitting Diodes. *Adv. Mater.* **2019**, *31*, 1904319.

(44) Leung, T. L.; Tam, H. W.; Liu, F.; Lin, J.; Ng, A. M. C.; Chan, W. K.; Chen, W.; He, Z.; Lončarić, I.; Grisanti, L.; Ma, C.; Wong, K. S.; Lau, Y. S.; Zhu, F.; Skoko, Ž.; Popović, J.; Djurišić, A. B. Mixed Spacer Cation Stabilization of Blue-Emitting n = 2 Ruddlesden−Popper Organic−Inorganic Halide Perovskite Films. *Adv. Opt. Mater.* **2020**, *8*, 1901679.

(45) Yang, X.; Zhang, X.; Deng, J.; Chu, Z.; Jiang, Q.; Meng, J.; Wang, P.; Zhang, L.; Yin, Z.; You, J. Efficient Green Light-Emitting Diodes Based on Quasi-Two-Dimensional Composition and Phase Engineered Perovskite with Surface Passivation. *Nat. Commun.* **2018**, *9*, 570.

(46) Shang, Y.; Liao, Y.; Wei, Q.; Wang, Z.; Xiang, B.; Ke, Y.; Liu, W.; Ning, Z. Highly Stable Hybrid Perovskite Light-Emitting Diodes Based on Dion-Jacobson structure. *Sci. Adv.* **2019**, *5*, No. eaaw8072.

(47) Ren, Z.; Xiao, X.; Ma, R.; Lin, H.; Wang, K.; Sun, X. W.; Choy, W. C. H. Hole Transport Bilayer Structure for Quasi-2D Perovskite Based Blue Light-Emitting Diodes with High Brightness and Good Spectral Stability. *Adv. Funct. Mater.* **2019**, *29*, 1905339.

(48) Xiao, Z.; Kerner, R. A.; Zhao, L.; Tran, N. L.; Lee, K. M.; Koh, T.-W.; Scholes, G. D.; Rand, B. P. Efficient Perovskite Light-Emitting Diodes Featuring Nanometre-Sized Crystallites. *Nat. Photonics* **2017**, *11*, 108−115.

(49) Wang, N.; Cheng, L.; Ge, R.; Zhang, S.; Miao, Y.; Zou, W.; Yi, C.; Sun, Y.; Cao, Y.; Yang, R.; Wei, Y.; Guo, Q.; Ke, Y.; Yu, M.; Jin, Y.; Liu, Y.; Ding, Q.; Di, D.; Yang, L.; Xing, G.; Tian, H.; Jin, C.; Gao, F.; Friend, R. H.; Wang, J.; Huang, W. Perovskite Light-Emitting Diodes Based on Solution-Processed Self-Organized Multiple Quantum Wells. *Nat. Photonics* **2016**, *10*, 699−704.

(50) Shang, Q.; Wang, Y.; Zhong, Y.; Mi, Y.; Qin, L.; Zhao, Y.; Qiu, X.; Liu, X.; Zhang, Q. Unveiling Structurally Engineered Carrier Dynamics in Hybrid Quasi-Two-Dimensional Perovskite Thin Films toward Controllable Emission. *J. Phys. Chem. Lett.* **2017**, *8*, 4431−4438.

(51) Liu, J.; Leng, J.; Wu, K.; Zhang, J.; Jin, S. Observation of Internal Photoinduced Electron and Hole Separation in Hybrid Two-Dimentional Perovskite Films. *J. Am. Chem. Soc.* **2017**, *139*, 1432−1435.

(52) Manser, J. S.; Kamat, P. V. Band filling with free charge carriers in organometal halide perovskites. *Nat. Photonics* **2014**, *8*, 737−743.

(53) Yang, S.; Dai, J.; Yu, Z.; Shao, Y.; Zhou, Y.; Xiao, X.; Zeng, X. C.; Huang, J. Tailoring Passivation Molecular Structures for Extremely Small Open-Circuit Voltage Loss in Perovskite Solar Cells. *J. Am. Chem. Soc.* **2019**, *141*, 5781−5787.

(54) Zhang, L.; Yang, X.; Jiang, Q.; Wang, P.; Yin, Z.; Zhang, X.; Tan, H.; Yang, Y. M.; Wei, M.; Sutherland, B. R.; Sargent, E. H.; You, J. Ultra-Bright and Highly Efficient Inorganic Based Perovskite Light-Emitting Diodes. *Nat. Commun.* **2017**, *8*, 15640.

(55) Cho, H.; Jeong, S.-H.; Park, M.-H.; Kim, Y.-H.; Wolf, C.; Lee, C.-L.; Heo, J. H.; Sadhanala, A.; Myoung, N.; Yoo, S.; Im, S. H.; Friend, R. H.; Lee, T.-W. Overcoming the Electroluminescence Efficiency Limitations of Perovskite Light-Emitting Diodes. *Science* **2015**, *350*, 1222−1225.

(56) Shi, D.; Adinolfi, V.; Comin, R.; Yuan, M.; Alarousu, E.; Buin, A.; Chen, Y.; Hoogland, S.; Rothenberger, A.; Katsiev, K.; Losovyj, Y.; Zhang, X.; Dowben, P. A.; Mohammed, O. F.; Sargent, E. H.; Bakr, O. M. Low Trap-State Density and Long Carrier Diffusion in Organolead Trihalide Perovskite Single Crystals. *Science* **2015**, *347*, 519−522.

(57) Chih, Y.-K.; Wang, J.-C.; Yang, R.-T.; Liu, C.-C.; Chang, Y.-C.; Fu, Y.-S.; Lai, W.-C.; Chen, P.; Wen, T.-C.; Huang, Y.-C.; Tsao, C.-S.; Guo, T.-F. NiO_x Electrode Interlayer and $CH_3NH_2/CH_3NH_3PbBr_3$ Interface Treatment to Markedly Advance Hybrid Perovskite-Based Light-Emitting Diodes. *Adv. Mater.* **2016**, *28*, 8687−8694.

(58) Wang, K.-H.; Peng, Y.; Ge, J.; Jiang, S.; Zhu, B.-S.; Yao, J.; Yin, Y.-C.; Yang, J.-N.; Zhang, Q.; Yao, H.-B. Efficient and Color-Tunable Quasi-2D $CsPbBr_xCl_{3-x}$ Perovskite Blue Light-Emitting Diodes. *ACS Photonics* **2019**, *6*, 667−676.

(59) Qu, X.; Zhang, N.; Cai, R.; Kang, B.; Chen, S.; Xu, B.; Wang, K.; Sun, X. W. Improving Blue Quantum Dot Light-Emitting Diodes by a Lithium Fluoride Interfacial Layer. *Appl. Phys. Lett.* **2019**, *114*, No. 071101.

(60) Zou, W.; Li, R.; Zhang, S.; Liu, Y.; Wang, N.; Cao, Y.; Miao, Y.; Xu, M.; Guo, Q.; Di, D.; Zhang, L.; Yi, C.; Gao, F.; Friend, R. H.; Wang, J.; Huang, W. Minimising Efficiency Roll-Off in High-Brightness Perovskite Light-Emitting diodes. *Nat. Commun.* **2018**, *9*, 608.

(61) Yang, M.; Wang, N.; Zhang, S.; Zou, W.; He, Y.; Wei, Y.; Xu, M.; Wang, J.; Huang, W. Reduced Efficiency Roll-Off and Enhanced Stability in Perovskite Light-Emitting Diodes with Multiple Quantum Wells. *J. Phys. Chem. Lett.* **2018**, *9*, 2038−2042.

(62) Yun, J. S.; Kim, J.; Young, T.; Patterson, R. J.; Kim, D.; Seidel, J.; Lim, S.; Green, M. A.; Huang, S.; Ho-Baillie, A. Humidity-Induced Degradation via Grain Boundaries of $HC(NH_2)_2PbI_3$ Planar Perovskite Solar Cells. *Adv. Funct. Mater.* **2018**, *28*, 1705363.

(63) Cho, H.; Kim, Y.-H.; Wolf, C.; Lee, H.-D.; Lee, T.-W. Improving the Stability of Metal Halide Perovskite Materials and Light-Emitting Diodes. *Adv. Mater.* **2018**, *30*, 1704587.